Articles

Contribution from the CNR—Centro di Studio per la Sintesi e la Struttura dei Composti dei Metalli di Transizione nei Bassi Stati di Ossidazione, Via G. Venezian 21, 20133 Milano, Italy, and Istituto di Chimica Strutturistica Inorganica, Via G. Venezian 21, 20133 Milano, Italy

Mixed Platinum–Rhodium Carbonyl Clusters. Synthesis, Reactivity, and Chemical Characterization of the $[PtRh_8(\mu_3\text{-}CO)_3(\mu\text{-}CO)_9(CO)_7]^{2-}$ Anion and X-ray Crystal Structure of Its Tetraethylammonium Salt

Alessandro Fumagalli,*[1a] Secondo Martinengo,[1a] Gianfranco Ciani,*[1b] and Giorgio Marturano[1b]

Received June 26, 1985

The anion $[PtRh_8(CO)_{19}]^{2-}$ has been synthesized by reaction of $[PtRh_4(CO)_{12}]^{2-}$ with $Rh_4(CO)_{12}$. It shows considerable reactivity toward CO, from which it is readily decomposed. The structure of the dianion has been determined by X-ray analysis of the tetraethylammonium salt. Crystal data: $C_{35}H_{40}N_2O_{19}PtRh_8$, M_r = 1811.0, orthorhombic, space group *Pmnb* [nonstandard setting of *Pnma* (No. 62)], a = 12.338 (3) Å, b = 16.340 (3) Å, c = 24.385 (8) Å, Z = 4; final R = 0.039, R_w = 0.052. The anion, of crystallographic C_s symmetry, shows a metallic skeleton that can be described as a stack of three triangles, generating two face-to-face condensed octahedra (the Pt atom being in the central triangle, in one of the positions of highest M–M connectivity); seven carbonyls, out of nineteen, are terminal, nine edge-bridging and three face-bridging. Variable-temperature ^{13}C NMR spectra show at room temperature complete scrambling of the carbonyls over the metallic frame with simultaneous coupling with all Rh and Pt atoms. At −100 °C a still partially dynamic situation is observed, which yields an ill-defined spectrum.

Introduction

In our previous studies on the synthesis of mixed Pt–Rh carbonyl clusters, we first obtained three low-nuclearity species, namely $[PtRh_5(CO)_{15}]^-$, $[PtRh_4(CO)_{14}]^{2-}$, and $[PtRh_4(CO)_{12}]^{2-}$,[2,3] and from their pyrolysis we have subsequently isolated some high-nuclearity clusters, such as $[Pt_2Rh_9(CO)_{22}]^{3-}$,[4] $[Pt_2Rh_{11}(CO)_{24}]^{3-}$, and $[PtRh_{12}(CO)_{24}]^{4-}$.[5,6] The pyrolytic process however, being a drastic one, yields generally only the more thermodynamically favored species, with little or no evidence of the intermediate growing steps, which are related to clusters of medium nuclearity. The aim of our present research is the isolation and the characterization of these unstable species, and we report the synthesis and complete chemical and structural characterization of a new species of intermediate nuclearity, the $[PtRh_8(CO)_{19}]^{2-}$ anion.

Results and Discussion

1. Synthesis and Reactivity of $[PtRh_8(CO)_{19}]^{2-}$. We discovered the first evidence of the $[PtRh_8(CO)_{19}]^{2-}$ dianion while attempting a rational synthesis of $[Pt_2Rh_9(CO)_{22}]^{3-}$[4,6] by reaction of $[PtRh_5(CO)_{15}]^-$[2,3] with $[PtRh_4(CO)_{12}]^{2-}$.[3] The reaction yielded a mixture of several products among which, after a fractional crystallization, the nine-metal dianion was found as a trace compound. We then attempted to obtain the new product in better yields through the redox condensation of $[PtRh_4(CO)_{12}]^{2-}$ with $Rh_4(CO)_{12}$.

The reaction was performed at room temperature with the $[NEt_4]^+$ salt. It appears to follow a complex path eventually yielding several products, among which four species have been identified: $[PtRh_8(CO)_{19}]^{2-}$ (I), $[PtRh_5(CO)_{15}]^-$ (II), $[Rh_{12}(CO)_{30}]^{2-}$ (III),[7] and an unknown brown anion (IV) with IR absorptions in MeCN at 1995 and 1820 cm^{-1}. Close IR monitoring of the reaction course shows that anions II and III are formed in the early stages. The former seems stable but the fate of anion III depends upon the solvent: when the reaction is performed in MeCN or in THF, anion III separates out as the poorly soluble $[NEt_4]^+$ salt and is thus present at the end of the reaction together with I, II, and IV. If acetone is used as a solvent, the $[NEt_4]^+$ salt of III is soluble, and the anion reacts further to give I. It is almost completely reacted in the final mixture.

The problem of the separation of $[PtRh_8(CO)_{19}]^{2-}$ has been solved by fractional crystallization based upon the different solubilities of the reaction products. The first separation is achieved as follows. The filtered reaction mixture is evaporated to dryness. The solids are extracted with THF, the mixture is filtered, and the resulting filtrate is treated with 2-propanol. This causes the salt $[NEt_4]_2[PtRh_8(CO)_{19}]$ to precipitate while $[NEt_4][PtRh_5(CO)_{15}]$ remains in the mother liquor. The precipitate is recrystallized from THF by the slow diffusion of 2-propanol carefully layered on the concentrated solution. This yields large black crystals of the product, sometimes together with small amounts of an insoluble black material resulting from decomposition of $[PtRh_8(CO)_{19}]^{2-}$ in solution, even under nitrogen atmosphere, during the week long recrystallization process.

The crystals are stable in air for many hours, while solutions are readily decomposed.

The IR spectra of $[NEt_4]_2[PtRh_8(CO)_{19}]$ show little dependence upon the solvent; in fact, while the spectrum in MeCN solution (Figure 1) shows broad bands in the CO stretching region at 2048 w, 2004–1998 s, and 1853 ms cm^{-1}, the only observable difference in THF and diglyme is the appearance of a weak shoulder at about 1825 cm^{-1}.

2. Reactivity under CO. The $[PtRh_8(CO)_{19}]^{2-}$ anion is decomposed under 1 atm of CO to give $[Rh_5(CO)_{15}]^-$,[8] $[PtRh_5(CO)_{15}]^-$, and $[PtRh_4(CO)_{14}]^{2-}$.

The presence of $[Rh_5(CO)_{15}]^-$ and $[PtRh_5(CO)_{15}]^-$ is clearly evidenced in the IR spectrum of the mixture, while the presence of $[PtRh_4(CO)_{14}]^{2-}$, whose IR absorptions are partially obscured by the two other anions, has been confirmed by addition, under CO, of [PPN]Cl[9] in 2-propanol followed by addition of heptane;

(1) (a) CNR. (b) Istituto di Chimica Strutturistica Inorganica.
(2) Fumagalli, A.; Martinengo, S.; Chini, P.; Albinati, A.; Bruckner, S.; Heaton, B. T. *J. Chem. Soc., Chem. Commun.* **1978**, 195.
(3) Fumagalli, A.; Martinengo, S.; Chini, P.; Galli, D.; Heaton, B. T., Della Pergola, R. *Inorg. Chem.* **1984**, *23*, 2947.
(4) Fumagalli, A.; Martinengo, S.; Ciani, G. *J. Organomet. Chem.* **1984**, *273*, C46.
(5) Fumagalli, A.; Martinengo, S.; Ciani, G. *J. Chem. Soc., Chem. Commun.* **1983**, 1381.
(6) Fumagalli, A.; Martinengo, S., unpublished results.
(7) Chini, P.; Martinengo, S. *Inorg. Chim. Acta* **1969**, *3*, 299.
(8) Fumagalli, A.; Koetzle, T. F.; Takusagawa, F.; Chini, P.; Martinengo, S.; Heaton, B. T. *J. Am. Chem. Soc.* **1980**, *102*, 1740.

0020-1669/86/1325-0592$01.50/0

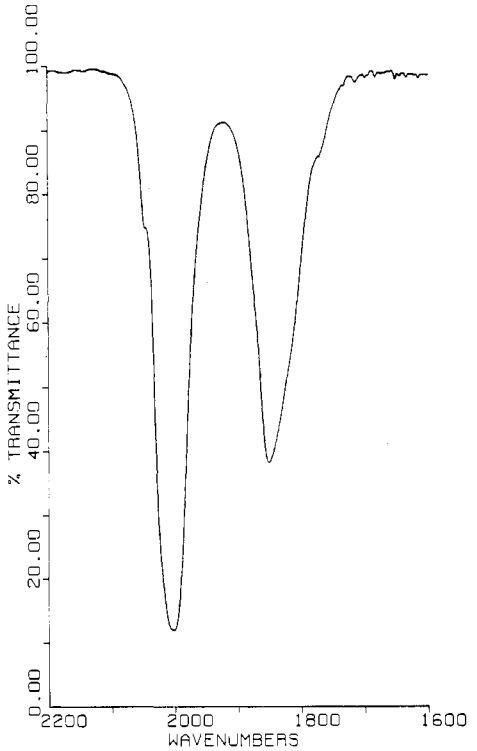

Figure 1. FT IR spectrum of $[NEt_4]_2[PtRh_8(CO)_{19}]$ in CH_3CN with solvent subtraction.

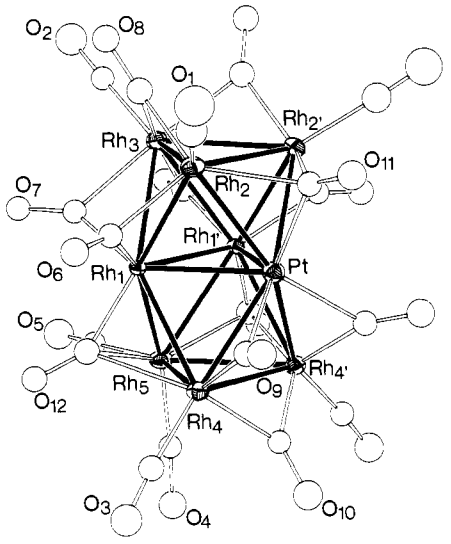

Figure 2. View of the dianion $[PtRh_8(\mu_3\text{-}CO)_3(\mu\text{-}CO)_9(CO)_7]^{2-}$. Primed atoms are related to unprimed ones by the crystallographic mirror plane passing through Pt, Rh(3), and Rh(5).

the resulting precipitate, dissolved in THF under CO, clearly shows the IR bands of $[PPN]_2[PtRh_4(CO)_{14}]$ in a mixture with a little amount of $[PPN][Rh_5(CO)_{15}]$. It is worth noting that the analogous homonuclear trianion $[Rh_9(CO)_{19}]^{3-}$[10] is also unstable under CO, yielding lower nuclearity species.

3. Structure of $[PtRh_8(CO)_{19}]^{2-}$. The structure of the dianion $[PtRh_8(CO)_{19}]^{2-}$ is illustrated in Figure 2. It possesses a rigorous crystallographically imposed, C_s-*m* symmetry, the mirror plane passing through the metal atoms Pt, Rh(3), and Rh(5). Bond distances and angles are given in Table I.

The metallic array is formed by two superimposed octahedral units sharing a face, as in the isoelectronic trianion $[Rh_9(CO)_{19}]^{3-}$.[10] The platinum atom occupies one of the vertices of the central triangle, thus attaining a higher metal–metal connectivity of 6 than the metals of the outer triangles (connectivity 4). The preference of Pt for cluster sites of higher metallic connectivity has already been observed in almost all the known Pt–Rh systems, i.e. in $[PtRh_{10}N(CO)_{21}]^{3-}$,[11] $[Pt_2Rh_9(CO)_{22}]^{3-}$,[4] $[Pt_2Rh_{11}(CO)_{24}]^{3-}$, and $[PtRh_{12}(CO)_{24}]^{4-}$,[5] and in other species that are presently under investigation.

The Pt–Rh and Rh–Rh bond lengths of mean values 2.730 and 2.779 Å, respectively, compare favorably with similar interactions

Table I. Bond Distances and Selected Angles in $[NEt_4]_2[PtRh_8(CO)_{19}]$

	Bond Distances (Å)		
Pt–Rh(1)	2.741 (2)	Rh(1)–Rh(4)	2.754 (2)
Pt–Rh(2)	2.717 (2)	Rh(1)–Rh(5)	2.752 (2)
Pt–Rh(4)	2.732 (2)	Rh(2)–Rh(2′)	2.860 (4)
Rh(1)–Rh(1′)	2.760 (2)	Rh(2)–Rh(3)	2.833 (3)
Rh(1)–Rh(2)	2.730 (2)	Rh(4)–Rh(4′)	2.778 (3)
Rh(1)–Rh(3)	2.767 (2)	Rh(4)–Rh(5)	2.806 (3)
Rh(2)–C(1)	1.89 (3)	Rh(3)–C(8)	2.16 (2)
Rh(3)–C(2)	1.89 (3)	Pt–C(9)	2.24 (2)
Rh(4)–C(3)	1.83 (2)	Rh(4)–C(9)	1.96 (2)
Rh(5)–C(4)	1.80 (3)	Rh(4)–C(10)	2.00 (2)
Rh(5)–C(5)	1.97 (3)	Pt–C(11)	2.09 (3)
Rh(1)–C(6)	2.01 (2)	Rh(2)–C(11)	2.26 (2)
Rh(2)–C(6)	2.05 (2)	Rh(1)–C(12)	1.93 (2)
Rh(1)–C(7)	1.89 (2)	Rh(4)–C(12)	2.42 (2)
Rh(3)–C(7)	2.17 (2)	Rh(5)–C(12)	2.39 (2)
Rh(2)–C(8)	1.94 (2)		
C(1)–O(1)	1.12 (3)	C(7)–O(7)	1.21 (2)
C(2)–O(2)	1.15 (3)	C(8)–O(8)	1.22 (2)
C(3)–O(3)	1.14 (2)	C(9)–O(9)	1.14 (2)
C(4)–O(4)	1.22 (3)	C(10)–O(10)	1.21 (3)
C(5)–O(5)	1.08 (3)	C(11)–O(11)	1.14 (3)
C(6)–O(6)	1.13 (2)	C(12)–O(12)	1.16 (2)
N(1)–C	1.46 (5)–1.64 (5)	N(2)–C	1.41 (6)–1.68 (10)
	Angles (deg)		
Rh(3)–Rh(2)–C(1)	145.3 (7)	Rh(4′)–Rh(4)–C(3)	136.8 (6)
Rh(2′)–Rh(2)–C(1)	127.7 (7)	Rh(1)–Rh(4)–C(3)	124.8 (6)
Rh(1)–Rh(2)–C(1)	141.2 (7)	Pt–Rh(4)–C(3)	157.2 (6)
Pt–Rh(2)–C(1)	124.3 (7)	Rh(4)–Rh(5)–C(4)	84.1 (8)
Rh(2)–Rh(3)–C(2)	135.4 (6)	Rh(1)–Rh(5)–C(4)	140.3 (5)
Rh(1)–Rh(3)–C(2)	135.8 (6)	Rh(4)–Rh(5)–C(5)	150.3 (1)
Rh(5)–Rh(4)–C(3)	112.4 (6)	Rh(1)–Rh(5)–C(5)	106.4 (7)
Rh(1)–C(6)–Rh(2)	84.3 (8)	Pt–C(11)–Rh(2)	77.3 (9)
Rh(1)–C(7)–Rh(3)	85.6 (7)	Rh(2)–C(11)–Rh(2′)	78.7 (10)
Rh(2)–C(8)–Rh(3)	87.3 (8)	Rh(1)–C(12)–Rh(4)	77.6 (7)
Pt–C(9)–Rh(4)	81.0 (7)	Rh(1)–C(12)–Rh(5)	78.3 (8)
Rh(4)–C(10)–Rh(4′)	88.2 (11)	Rh(4)–C(12)–Rh(5)	71.2 (6)
C(9)–Pt–C(9′)	98.2 (10)	C(2)–Rh(3)–C(8)	92.4 (8)
C(9)–Pt–C(11)	106.5 (7)	C(7)–Rh(3)–C(7′)	88.9 (10)
C(6)–Rh(1)–C(7)	94.3 (8)	C(8)–Rh(3)–C(8′)	82.6 (11)
C(6)–Rh(1)–C(12)	99.7 (8)	C(3)–Rh(4)–C(9)	103.6 (8)
C(7)–Rh(1)–C(12)	97.7 (8)	C(3)–Rh(4)–C(10)	95.8 (8)
C(1)–Rh(2)–C(6)	94.8 (9)	C(3)–Rh(4)–C(12)	85.8 (7)
C(1)–Rh(2)–C(8)	95.9 (9)	C(9)–Rh(4)–C(10)	93.7 (9)
C(1)–Rh(2)–C(11)	90.1 (9)	C(4)–Rh(5)–C(5)	98.1 (11)
C(6)–Rh(2)–C(8)	97.5 (8)	C(4)–Rh(5)–C(12)	104.3 (5)
C(2)–Rh(3)–C(7)	92.8 (8)	C(5)–Rh(5)–C(12)	96.3 (5)
Rh(2)–C(1)–O(1)	175 (2)	Rh(3)–C(8)–O(8)	129 (2)
Rh(3)–C(2)–O(2)	177 (3)	Pt–C(9)–O(9)	126 (2)
Rh(4)–C(3)–O(3)	174 (2)	Rh(4)–C(9)–O(9)	152 (2)
Rh(5)–C(4)–O(4)	175 (2)	Rh(4)–C(10)–O(10)	135.9 (5)
Rh(5)–C(5)–O(5)	179 (2)	Pt–C(11)–O(11)	133 (2)
Rh(1)–C(6)–O(6)	140 (2)	Rh(2)–C(11)–O(11)	134 (1)
Rh(2)–C(6)–O(6)	135 (2)	Rh(1)–C(12)–O(12)	148 (2)
Rh(1)–C(7)–O(7)	144 (1)	Rh(4)–C(12)–O(12)	128 (1)
Rh(3)–C(7)–O(7)	130 (1)	Rh(5)–C(12)–O(12)	124 (1)
Rh(2)–C(8)–O(8)	143 (2)		

(9) $[PPN]^+ = [(Ph_3P)_2N]^+$, (μ-nitrido)bis(triphenylphosphorus)(1+).

(10) Martinengo, S.; Fumagalli, A.; Bonfichi, R.; Ciani, G.; Sironi, A. *J. Chem. Soc., Chem. Commun.* **1982**, 825.

(11) Martinengo, S.; Ciani, G.; Sironi, A. *J. Am. Chem. Soc.* **1982**, *104*, 328.

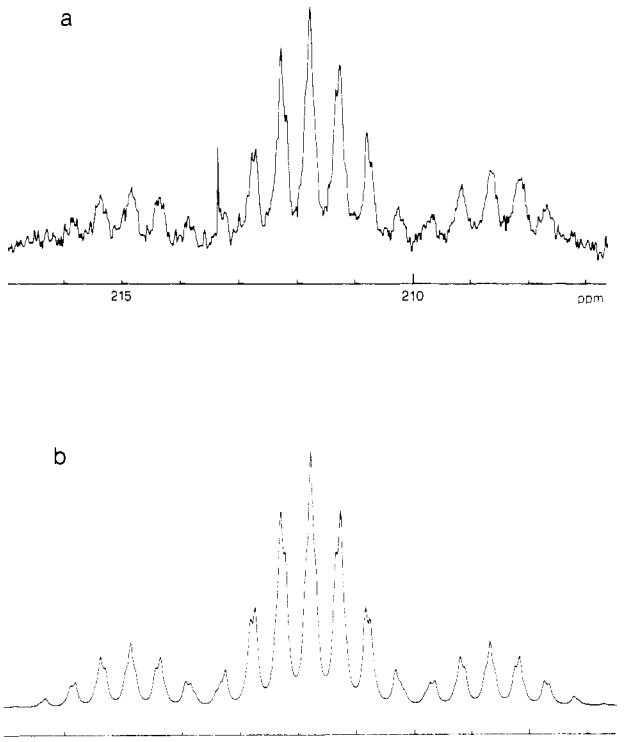

Figure 3. (a) ^{13}C NMR spectrum of $[NEt_4]_2[PtRh_8(CO)_{19}]$ (carbonyl region) in THF-d_8 at room temperature. (b) Simulated spectrum with J_{C-Rh} = 8.7 Hz (triplet), J_{C-Rh} = 10.5 Hz (septet), J_{C-Pt} = 125.7 Hz (satellites), and $W_{1/2}$ = 2 Hz.

in other cluster compounds. This mean Pt–Rh bond length is intermediate between the shorter average bond distances in $[Pt_2Rh_9(CO)_{22}]^{3-}$ (2.707 Å) and in $[PtRh_{10}N(CO)_{21}]^{3-}$ (2.711 Å) and the longer ones in $[PtRh_{12}(CO)_{24}]^{4-}$ (2.776 Å) and in $[PtRh_5(CO)_{15}]^-$ (2.790 Å).[2]

Within the central triangle the metal–metal bonds [Pt–Rh(1) = 2.741 (2) Å, Rh(1)–Rh(1′) = 2.760 (2) Å] are somewhat longer than the corresponding mean Rh–Rh interactions in $[Rh_9(CO)_{19}]^{3-}$ (2.728 Å). The other M–M bonds, as well as the ligand stereochemistries are essentially similar in the two species.

The mean values of the Rh–C and C–O bonds for the seven terminal carbonyls are 1.87 and 1.14 Å, respectively. Of the nine edge-bridging groups, only three are almost symmetric, on the edges Rh(1)–Rh(2), Rh(1′)–Rh(2′), and Rh(4)-Rh(4′) (mean Rh–C and C–O are 2.02 and 1.16 Å). The four groups bound to Rh(3) show significantly longer Rh(3)–C bonds (mean 2.16 Å vs. 1.92 Å for the other Rh–C bonds). Interestingly, the remaining two doubly bridging groups, bound to Pt, exhibit Pt–C bond lengths much longer (2.24 Å) than the Rh–C ones (1.96 Å), unlike the Rh_9 species (corresponding mean interactions of 2.06 and 1.98 Å, respectively).

The three triply bridging carbonyls are also here quite asymmetric, that bound to Pt showing a certain lengthening of the Pt–C distance (2.09 Å) with respect to the analogous Rh–C interaction in the Rh_9 trianion (1.99 Å). This pattern of Pt–C bonds agrees with the lower need of electrons of Pt with respect to Rh.

4. ^{13}C NMR spectra were obtained for a sample of $[NEt_4]_2[PtRh_8(CO)_{19}]$, ca. 25% ^{13}CO enriched, prepared from preenriched reactants. At room temperature this showed a complex multiplet at 211.7 ppm in the carbonyl region, consistent with complete fluxionality of all the carbonyls over the metallic skeleton (Figure 3a). This multiplet fits well with the simulated spectrum of Figure 3b, consistent with a triplet of septets, with the satellite resonances (J = 125.7 ± 0.5 Hz) due to the active ^{195}Pt isotope (natural abundance 33.8%). With reference to Figure 2, the triplet (J = 8.7 ± 0.5 Hz) appears clearly due to the coupling with the two equivalent Rh(1) and Rh(1′) atoms of the middle triangle, while the septet (10.5 ± 0.5 Hz) has to be assigned to the six Rh atoms in the outer triangles. It has to be noted, however, that, on the basis of the metal skeleton as depicted in Figure 2, and though the carbonyls' fluxionality increases the anion symmetry, the Rh atoms of the external triangles should be divided into two groups of two and four magnetically equivalent atoms, respectively Rh(3), Rh(5) and Rh(2), Rh(2′), Rh(4), Rh(4′), and their expected contribution should be a triplet of quintets. The result obtained suggests two hypotheses: (a) the coupling constants involving the carbons are nearly the same for the two kinds of Rh's, or (b) all six Rh atoms, in solution at room temperature, are magnetically equivalent due to a fluxional process of the metallic skeleton, consistent with a free rotation along a pseudo-threefold axis, analogous to that found in the Pt_3 oligomers $[Pt_3(CO)_6]_n^{2-}$ (n = 2–5).[12]

At −50 °C a single broad resonance at 212.3 ppm is still present, and even on lowering of the temperature to about −100 °C (close to the freezing point of the solution) there is still indication of partial fluxionality, although the resonances now appear spread, as very broad signals, over the range 180–250 ppm. Thus no assignment could be made with reference to the solid-state structure.

Experimental Section

All the reactions and subsequent manipulations were carried out under nitrogen atmosphere in solvents carefully purified and stored under nitrogen. $[NEt_4]_2[PtRh_4(CO)_{12}]$ and $Rh_4(CO)_{12}$ were prepared according to the literature.[3,13]

^{13}CO-enriched samples (to ca. 20–30%) were prepared from $[NEt_4]_2[PtRh_4(CO)_{12}]$ (previously enriched by direct exchange at room temperature with 90% ^{13}CO using standard vacuum-line techniques) and unenriched $Rh_4(CO)_{12}$, according to method 1.

^{13}C NMR spectra were recorded on both Bruker WP80 and Varian XL-200 multinuclear spectrophotometers in THF-d_8 solution under nitrogen. The spectrum of Figure 3a was obtained on the Bruker WP80 instrument with a resolution of 0.244 Hz.

Infrared spectra were recorded on a Perkin-Elmer 781 grating spectrophotometer and on a Nicolet MX-1 FT IR instrument with subtraction of the solvent, using 0.1-mm calcium fluoride cells previously purged with nitrogen.

1. Synthesis of $[NEt_4]_2[PtRh_8(CO)_{19}]$. $[NEt_4]_2[PtRh_4(CO)_{12}]$ (357.7 mg, 0.297 mmol) and $Rh_4(CO)_{12}$ (231 mg, 0.309 mmol) were placed, under nitrogen, in a Schlenk tube, and acetone (20 mL) was added. The mixture was stirred at room temperature for about 48 h and then evaporated under vacuum. The residue was treated with THF (15 mL), which extracted part of the mixture, leaving an insoluble tacky residue; the solution was filtered on a glass frit and the residue discharged. After addition of 2-propanol (30 mL) the solution was concentrated under vacuum to about 25–30 mL to give a microcrystalline precipitate. The precipitate was filtered out, washed with 2-propanol (5 + 5 mL), and vacuum-dried, while the brown mother liquor, containing for the most part the byproduct $[NEt_4][PtRh_5(CO)_{15}]$, was discarded. The crude product was dissolved in THF (5 mL); the mixture was filtered from a little amount of insoluble material, and the filtrate was carefully layered with 2-propanol to give, after about a week of slow diffusion, a product consisting mostly of nice black crystals of $[NEt_4]_2[PtRh_8(CO)_{19}]$. Yield: 182 mg (34%).

Anal. Found (calcd): C, 21.85 (23.21); H, 2.33 (2.23); N, 1.48 (1.55).

Should the above crude product be very impure (as evidenced by extra bands with respect to the IR spectrum of Figure 1), an additional purification procedure can be performed by extraction with diglyme (15 mL), filtration of the insoluble material, and addition into the clear solution of hexane (20 mL); this yields a tacky precipitate, which is isolated from the mother liquor after decantation with a syringe, washed with hexane (5 mL), and vacuum-dried. Redissolution of this material with THF gives a solution that can be layered with 2-PrOH as above.

2. Reaction of $[NEt_4]_2[PtRh_8(CO)_{19}]$ with CO. $[NEt_4]_2[PtRh_8(CO)_{19}]$ (45.8 mg, 0.025 mmol) was dissolved, under nitrogen, in THF (5 mL). The vessel was briefly evacuated and refilled with CO. IR monitoring showed complete decomposition after ca. 20 h and clear evidence of $[NEt_4][Rh_5(CO)_{15}]$ and $[NEt_4][PtRh_5(CO)_{15}]$ (bands at 2040 s, 2005 vs, 1870 m, 1840 ms, and 1785 m cm^{-1} and at 2040 s and 1785 ms cm^{-1}, respectively). After addition of [PPN]Cl (30 mg in 6 mL of 2-propanol) and separation of a small amount of black precipitate, the resulting solution was treated with heptane (15 mL) while being stirred to give a precipitate, which after decantation and removal of the mother liquor was

(12) Brown, C.; Heaton, B. T.; Towl, A. D. C.; Chini, P.; Fumagalli, A.; Longoni, G. *J. Organomet. Chem.* **1979**, *181*, 233.
(13) Martinengo, S.; Giordano, G.; Chini, P. *Inorg. Synth.* **1980**, *20*, 209.

Table II. Final Positional Parameters

atom	*x*	*y*	*z*
Pt	0.250	0.23216 (9)	0.13071 (5)
Rh(1)	0.1381 (1)	0.2304 (1)	0.03358 (6)
Rh(2)	0.1341 (2)	0.0976 (1)	0.10153 (7)
Rh(3)	0.250	0.0917 (2)	0.0013 (1)
Rh(4)	0.1374 (2)	0.3680 (1)	0.09875 (7)
Rh(5)	0.250	0.3665 (2)	−0.0012 (1)
C(1)	0.040 (2)	0.040 (2)	0.149 (1)
O(1)	−0.009 (2)	0.003 (1)	0.1784 (9)
C(2)	0.250	0.023 (2)	−0.061 (1)
O(2)	0.250	−0.022 (2)	−0.098 (1)
C(3)	0.029 (2)	0.445 (1)	0.1000 (9)
O(3)	−0.032 (2)	0.497 (1)	0.1021 (7)
C(4)	0.250	0.476 (2)	0.007 (1)
O(4)	0.250	0.551 (2)	0.008 (1)
C(5)	0.250	0.363 (2)	−0.082 (1)
O(5)	0.250	0.360 (2)	−0.126 (1)
C(6)	0.014 (2)	0.171 (1)	0.0697 (9)
O(6)	−0.075 (1)	0.178 (1)	0.0772 (6)
C(7)	0.373 (2)	0.172 (1)	−0.0330 (9)
O(7)	0.417 (1)	0.1704 (9)	−0.0773 (6)
C(8)	0.135 (2)	0.016 (1)	0.0439 (9)
O(8)	0.093 (1)	−0.0483 (9)	0.0294 (6)
C(9)	0.113 (2)	0.305 (1)	0.1659 (9)
O(9)	0.066 (1)	0.291 (1)	0.2053 (6)
C(10)	0.250	0.439 (2)	0.133 (1)
O(10)	0.250	0.498 (2)	0.164 (1)
C(11)	0.250	0.120 (2)	0.172 (1)
O(11)	0.250	0.102 (1)	0.217 (1)
C(12)	0.064 (2)	0.328 (1)	0.0104 (9)
O(12)	−0.007 (1)	0.3578 (9)	−0.0138 (6)
N(1)	0.250	0.170 (2)	−0.290 (1)
C(101)	0.189 (4)	0.161 (3)	−0.343 (2)
C(102)	0.314 (4)	0.258 (3)	−0.290 (2)
C(103)	0.341 (4)	0.102 (3)	−0.289 (2)
C(104)	0.189 (4)	0.158 (4)	−0.239 (2)
C(105)	0.250	0.158 (2)	−0.393 (2)
C(106)	0.250	0.331 (3)	−0.298 (2)
C(107)	0.286 (4)	0.018 (3)	−0.281 (2)
C(108)	0.250	0.168 (2)	−0.184 (2)
N(2)	0.250	−0.242 (1)	0.1377 (9)
C(201A)	0.372 (5)	−0.237 (4)	0.151 (3)
C(202A)	0.214 (5)	−0.279 (4)	0.081 (3)
C(203A)	0.207 (7)	−0.154 (6)	0.135 (4)
C(204A)	0.195 (7)	−0.303 (6)	0.175 (3)
C(205A)	0.041 (8)	−0.309 (6)	0.140 (4)
C(201B)	0.377 (8)	−0.278 (6)	0.130 (4)
C(202B)	0.250	−0.194 (5)	0.087 (3)
C(203B)	0.250	−0.195 (4)	0.186 (3)
C(204B)	0.199 (8)	−0.324 (6)	0.138 (4)
C(205B)	0.052 (7)	−0.286 (5)	0.177 (3)
C(206)	0.250	−0.231 (3)	0.033 (2)
C(207)	0.208 (3)	−0.111 (2)	0.196 (2)
C(208)	0.427 (4)	−0.321 (3)	0.166 (2)

redissolved in THF (ca. 0.5 mL). IR spectra, recorded under CO atmosphere, showed the presence of $[PPN]_2[PtRh_4(CO)_{14}]$ (bands at 1995 s, 1962 s, 1807 m, 1800 m, and 1750 m cm^{-1}) together with a small amount of $[PPN][Rh_5(CO)_{15}]$.

3. X-ray Analysis. Crystal Data: $C_{35}H_{40}N_2O_{19}PtRh_8$, M_r = 1811.0, orthorhombic, space group *Pmnb* [nonstandard setting of *Pnma* (No. 62)], a = 12.338 (3) Å, b = 16.340 (3) Å, c = 24.385 (8) Å, V = 4916.1 Å^3, D_c = 2.45 g cm^{-3} for Z = 4, $F(000)$ = 3416; Mo Kα radiation (λ = 0.71073 Å), μ(Mo Kα) = 55.08 cm^{-1}.

Intensity Measurements. A crystal sample of dimensions 0.15 × 0.17 × 0.18 mm was mounted on a glass fiber in the air and transferred to an automated Enraf-Nonius CAD4 diffractometer. The setting angles of 25 random intense reflections ($16 < 2\theta < 25°$) were used to determine by least-squares fit accurate cell constants and orientation matrix. The data collection, using graphite-monochromated Mo K_α radiation, was performed by the ω-scan method, within the limits $3 < \theta < 24.5°$. A variable scan speed (from 2 to 20°/min) and variable scan range of (1.0 + 0.35 tan θ)° were used, with a 25% extension at each end of the scan range for background determination. The total number of collected reflections was 4474. The intensities of three standard reflections were measured every 2 h, and no significant decay was observed. The intensities were corrected for Lorentz and polarization effects. An empirical absorption correction was applied, on the basis of ψ-scans (ψ 0–360° every 10°) of suitable reflections with χ values close to 90°; the maximum, minimum, and average relative transmission values were 1.00, 0.94, and 0.96, respectively. A set of 1484 independent significant reflections, with $I > 3\sigma(I)$, was used in the structure solution and refinements.

Structure Solution and Refinements. All computations were performed on a PDP 11/34 computer, using the Enraf-Nonius Structure Determination Package (SDP) and the physical constants tabulated therein. The structure was solved by Patterson and Fourier methods. Both anions and cations lie in special positions on a crystallographic mirror plane. This location causes the cations to be disordered. In the first cation, containing N(1), the four methylene carbon atoms (C(101)–C(104)) are doubled by the mirror plane, resulting in a distorted cube of half carbon atoms; also one of the methyl carbons (C(107)) is doubled by the same plane, while the other three carbons are not disordered, lying on the plane. The other cation, containing N(2), exhibits a more complex disorder: eight independent peaks were observed, bound to the nitrogen atom. The methylene atoms were treated as belonging to two differently oriented models (A and B), each further disordered by the mirror plane (C atomic fraction 0.25). The same situation was observed also for two external carbons (C(205A) and C(205B), bound to C(201A) and C(201B), respectively), while for the remaining methyl carbons three atoms with fraction 0.50 were refined (C(206), C(207), and C(208)), each corresponding to a pair of coincident atoms of the two models.

The refinements were carried out by full-matrix least-squares methods. Anisotropic thermal parameters were assigned to the metal atoms (Pt and Rh) only. The final values of the conventional R and R_w factors were 0.039 and 0.052, respectively. Weights were assigned according to the formula $w = 1/\sigma^2(F_o)$, with $\sigma(F_o) = \sigma(F_o^2)/2F_o$ and $\sigma(F_o^2) = [\sigma^2(I) + (AI)^2]^{1/2}/L_p$, the fudge factor A being assumed equal to 0.03. The final difference-Fourier map showed some residual peaks not exceeding ca. 1.0 e/Å^3.

The final positional parameters are reported in Table II.

Acknowledgment. We thank Ms. M. Bonfà of Università di Milano for recording the NMR spectra.

Registry No. $[NEt_4]_2[PtRh_8(CO)_{19}]$, 100102-32-7; $[NEt_4]_2[PtRh_4(CO)_{12}]$, 100082-40-4; $Rh_4(CO)_{12}$, 19584-30-6; Pt, 7440-06-4; Rh, 7440-16-6.

Supplementary Material Available: A table of thermal parameters and a list of computed and observed structure factor moduli (12 pages). Ordering information is given on any current masthead page.